Inhibition of Cancer Cell Migration by Multiwalled Carbon Nanotubes

*Lorena García-Hevia, Rafael Valiente, José L. Fernández-Luna, Emmanuel Flahaut, Lidia Rodríguez-Fernández, Juan C. Villegas, Jesús González, and Mónica L. Fanarraga**

Finding ways to control cancer at the primary site means the difference between life and death. Localized tumors can be eliminated by surgery and radiation therapy, and as a general rule do not represent a life-threatening problem. However, when cancer spreads to other tissues it becomes an incurable condition where treatments can only delay the progression of the disease and prolong survival.

Carbon nanotubes (CNTs) represent a highly versatile heterogeneous family of nanomaterials that display interesting physico-chemical properties.[1] These nanomaterials are well known to interact with the biological matter, penetrating inside tissues and cells,[2,3] leading to a plethora of side effects in living organisms.[4–7] *In vitro*, CNTs can be actively captured by most cells.[2,3] Once inside the cells, CNTs also intermingle with many subcellular structures at nanoscale, mostly filaments such as DNA,[8] actin,[9,10] or microtubules.[5,11] In particular, multiwalled carbon nanotubes (MWCNTs) have been shown to contact cell surface receptors,[2] translocate across cell membranes via the endocytic pathway in both, phagocytic and nonphagocytic cells,[2,3] and interfere with the microtubule function triggering antiproliferative and pro-apoptotic effects.[5,10,11]

MWCNTs display interesting biomimetic properties with microtubules.[11-13] These cytoskeletal elements are intracellular protein nanotubes that result from the self-association of tubulin into 4 nm polymers, known as protofilaments.[14] Tubulin protofilaments are organized into a circle assembling a 25 nm diameter tube, the microtubule (Figure S1, Supporting Information). Thus, MWCNTs and microtubules are both 1D hollow nanofilaments with a similar length-to-diameter ratio, resiliency, self-assembly properties, and a comparable surface reactivity[12] that favors their association into biosynthetic polymers both, *in vitro*[13] and *in vivo*.[11] There is however, a big difference between these two nanofilaments that has chief biotechnological implications. While CNTs are very stable filaments, microtubules are highly dynamic polymers that stochastically switch between phases of polymerization–depolymerization on the time scale of seconds both, *in vitro* and *in vivo*.[15] During mitosis, the microtubule dynamic behavior increases 20- to 100-fold to assemble the so-called "mitotic spindle", a microtubule-based structure responsible for the balanced segregation of the chromosomes between the daughter cells.[15,16] Some of the most widely used antineoplastic drugs such as paclitaxel (taxol) and their derivatives are microtubule-binding chemicals that behave as spindle poisons, inhibiting cell proliferation, leading to mitotic arrest and cell death.[17–19]

MWCNTs interact tubulin intracellularly assembling biosynthetic filaments.[11] These hybrid microtubules display a significantly enhanced stability compared to the standard tubulin polymers that favors noncentrosomal cytoplasmic microtubule nucleation. As the word "centrosome" means, this structure is a key organizer of the microtubule cytoskeleton in the cell, participating in all cellular activities including cell division and migration. CNT-triggered centrosomal abnormalities are well documented in the literature. These include aberrant mitotic spindle assemblies, chromosomal malsegregation, abnormal interphase microtubule arrays, and cytotoxicity in general.[5,11,19] Since centrosomal positioning is a key structure in migrating cells, conferring membrane and cytoskeletal directionality, here we determine if MWCNTs have the intrinsic ability to hinder cancer cell spreading and discuss the molecular mechanics behind this effect.

For the study we first determined the position and trajectory of the centrosome in migrating HeLa cells treated with MWCNTs. As a rule of thumb, migrating cells display a polarized morphology[20] determined by the so-called, nuclear-centrosomal axis (**Figure 1**A). This axis, first identified by Van Beneden in the 1880s,[21] contributes to the asymmetric organization of

L. García-Hevia
Departamento de Biología Molecular
Universidad de Cantabria-IDIVAL
39011 Santander, Spain
Dr. R. Valiente
Departamento de Física Aplicada
Facultad de Ciencias
Universidad de Cantabria-IDIVAL
39005 Santander, Spain
Dr. J. L. Fernández-Luna
Hospital Valdecilla-IDIVAL
39011 Santander, Spain
Dr. E. Flahaut
CNRS, Institut Carnot CIRIMAT
Université de Toulouse
F-31062 Toulouse, France
Dr. L. Rodríguez-Fernández
SERMET
Universidad de Cantabria
39005 Santander, Spain
Dr. J. C. Villegas
Departamento de Anatomía y Biología Celular
Universidad de Cantabria-IDIVAL
39011 Santander, Spain
Dr. J. González
MALTA-Consolider Team, CITIMAC, Facultad de Ciencias
Universidad de Cantabria-IDIVAL
39005 Santander, Spain
Dr. M. L. Fanarraga
Departamento de Biología Molecular
Universidad de Cantabria-IDIVAL
39011 Santander, Spain
E-mail: fanarrag@unican.es

DOI: 10.1002/adhm.201500252

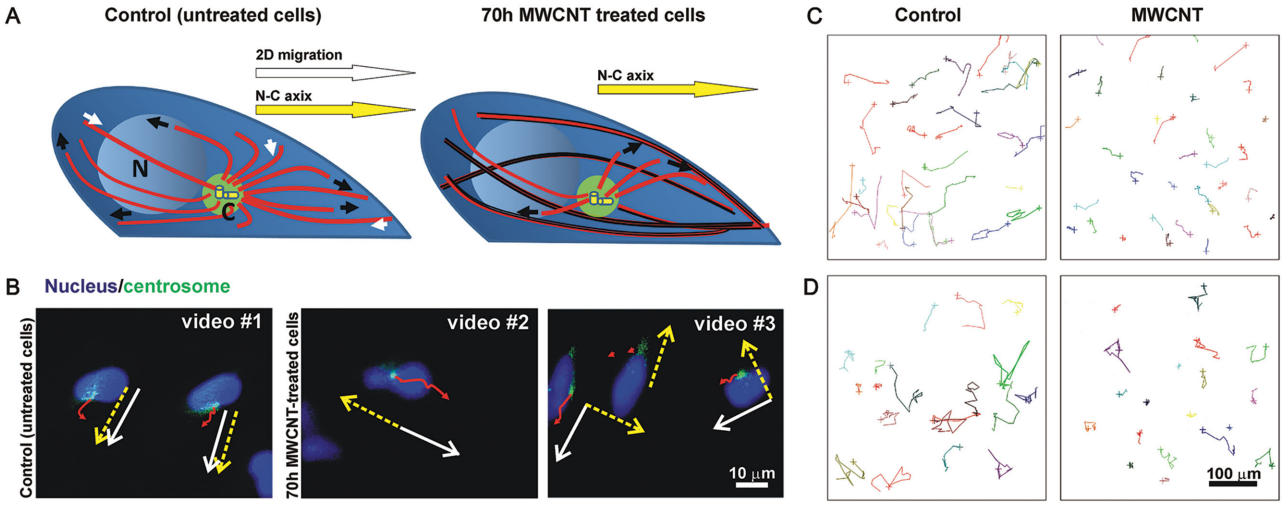

Figure 1. MWCNTs produce centrosomal mispositioning and disrupt the nuclear–centrosomal axis hindering cell migration. A) Diagram of the disposition of the nucleus (N), centrosome (C, green), and microtubule array (red filaments) in control and MWCNT-treated (MWCNTs in black) migrating cells. Microtubule traction forces are also represented (small white and black arrows). The cell polarity and migratory direction (white arrow) relative to the nuclear–centrosomal axis (yellow arrow) is indicated. B) Frozen live-cell images obtained from time-lapse videos S1–S3 (Supporting Information) of migrating HeLa cells displaying labeled nuclei (blue) and centrosomes (green). The centrosomal trajectories (red arrows), average cell trajectories (white arrows), and nuclear–centrosomal axes (yellow arrows) are shown for MWCNT-treated cells and untreated controls. C,D) Representative glioblastoma (U87MG) and neuroblastoma (SH-SY5Y) 5 h cell tracking trajectories, respectively. Cultures grown in the absence (control) or presence of MWCNTs were recorded during 70 h. Individual cell trajectories indicated by colored lines, are shorter in cells incubated with MWCNTs.

cell structure during migration, and corresponds to the final direction of the displacement.[22] Microtubules, connected to the migrating front of the cell, pull forward the centrosome dragging the nucleus forward, thus redistributing the traction forces generated at the cell's migrating front, to the centrosome, and throughout the cytoplasm to produce an effective net cell body translation. Accordingly, in cells migrating on 2D substrates, the centrosome is typically positioned between the nucleus and the leading edge, along this axis. To determine the orientation of nuclear-centrosomal axis we performed time-lapse video microscopy on live HeLa cells displaying fluorescently labeled centrosomes and nuclei (Experimental section). This allowed comparing this axis with the direction of the cell trajectory in migrating MWCNT-treated cells and untreated controls. As summarized in Figure 1B, in frozen live-cell images obtained from Videos S1–S3 (Supporting Information), the centrosomes in MWCNT-treated cells displayed a random perinuclear location and were aberrantly positioned with respect to the nuclear trajectory. As a result, in MWCNT-treated cells the direction of the cell migration (white arrows) and the nuclear–centrosomal axes (yellow arrows) were not parallel. Conversely, in untreated-control HeLa cells centrosomes were located along the nuclear–centrosomal axis, between the nucleus and the leading edge of the cells, just as described by Van Beneden.[21]

To investigate the consequences of these findings, we calculated the average migration speed of control and MWCNT-treated cells using cell tracking analysis (Experimental Section). For the study we investigated various cancer cell lines including: (i) HeLa cells; (ii) MCF7 cells, a human breast cancer cell line; (iii) SH-SY5Y cells, a neuroblastoma cell line originally established from a metastatic tumor; and (iv) U87MG cells, a grade IV human glioma cell line. Cells were incubated with 25 μg mL^{-1} MWCNTs for 70 h and were time-lapse video recorded for 5 h. This MWCNT concentration produced no obvious signs of toxicity but revealed a reduction of more than 40% in the average speed of HeLa cells treated with MWCNTs. A statistically significant cell speed reduction was also shown for the other two fast-migrating cancer cell lines, SH-SY5Y and U87MG when exposed to MWCNTs (**Table 1**, and Figure 1C,D). A possible interference with MWCNTs settled on the growing matrix was also considered. However, under our functionalization conditions MWCNTs precipitation or aggregation on the growing matrix is never observed. Besides, recent studies have shown that CNTs facilitate cell migration.[23]

To further demonstrate our hypothesis we decided to replicate this experiment on real tumor cells isolated from surgical specimens. Characteristically, tumor explant derived cancer cells are much more heterogeneous than most cancer cell line models. We chose glioblastoma multiforme cells (GBM) for the study because these cells typically infiltrate the surrounding brain tissue leading to tumor recurrence after surgery. Glioblastomas are the most common and aggressive primary brain tumor in adults, and have an unfavorable prognosis with a median survival time of less than 15 months, mostly due to recurrence. For the study we isolated GBM cells from surgical specimens that were fully characterized[24] before exposure to 25 μg mL^{-1} MWCNTs for 70 h. This experiment served to confirm that MWCNTs also triggered a significant antimigratory effect (18% speed reduction) in real tumor-derived cells (**Figure 2**A, Table 1).

The presence of intracellular MWCNTs in GBM cells was confirmed using confocal Raman spectroscopy focusing the laser within the cell's cytoplasm. We observed differences in the peak positions in the spectrum of intracellular MWCNTs, slightly shifted to higher wavenumbers (Figure 2B, inset), together with a decrease in Raman intensities of the D, G, and G′

DOI: 10.1002/adhm.201500252

Table 1. Migration inhibitory effect of MWCNTs for different cancer cells types.

Cell type	Control speed[a)]	MWCNT speed[a)]	Speed reduction [%]	DF[b)]	t/p[c)]	% Statistical significance
HeLa	12.7 ± 0.6	7.4 ± 0.4	41	245	$7.2/<10^{-10}$	>99.99
MCF7	1.6 ± 0.1	1.5 ± 0.1	6	130	0.4/0.64	NS
SH-SY5Y	8.7 ± 0.7	6.8 ± 0.4	22	114	2.3/0.02	95–98
U87MG	8.5 ± 0.2	6.1 ± 0.2	28	249	$7.1/<10^{-10}$	>99.99
GBM	9.2 ± 0.2	7.5 ± 0.1	18.5	408	$6.5/<10^{-9}$	>99.99

[a)]Average speed is shown in nm s^{-1}; [b)]DF = degrees of freedom; [c)]t/p = Student's t-test and p probability.

modes (Figure 2B and Table S1, Supporting Information). As it has been previously shown, CNTs exhibit variations in the relative Raman intensities and/or positions for various Raman modes depending on different physical[25] or chemical[26,27] environments and according to their agglomeration state. In this study, functionalized intracellular MWCNTs display a well-pronounced G mode indicative of a significant dispersion. The overall data also indicated that the coating of MWCNTs did not significantly affect the G mode profile, as previously reported for noncovalently modified SWCNTs dispersed in aqueous solutions containing peptides[25–31] or proteins.[32,33] The precise cytoplasmic distribution of the intracellular MWCNTs was also determined on a single confocal Z-plane obtained across the GBM cell cytoplasm using confocal Raman imaging, following the G band at 1586 cm^{-1} (Figure 2C,D). This technique revealed how intracellular MWCNTs were localized in small spots throughout the cytoplasm, a distribution coinciding with that previously described in MWCNT-treated cell lines.[11] These experiments demonstrate how MWCNTs can also translocate inside surgical specimen–derived cancer cells, and how these nanomaterials can also hinder GBM cell spreading.

Finally, we also explored if the observed antimigratory effect was dose-dependent. For the study we treated all the

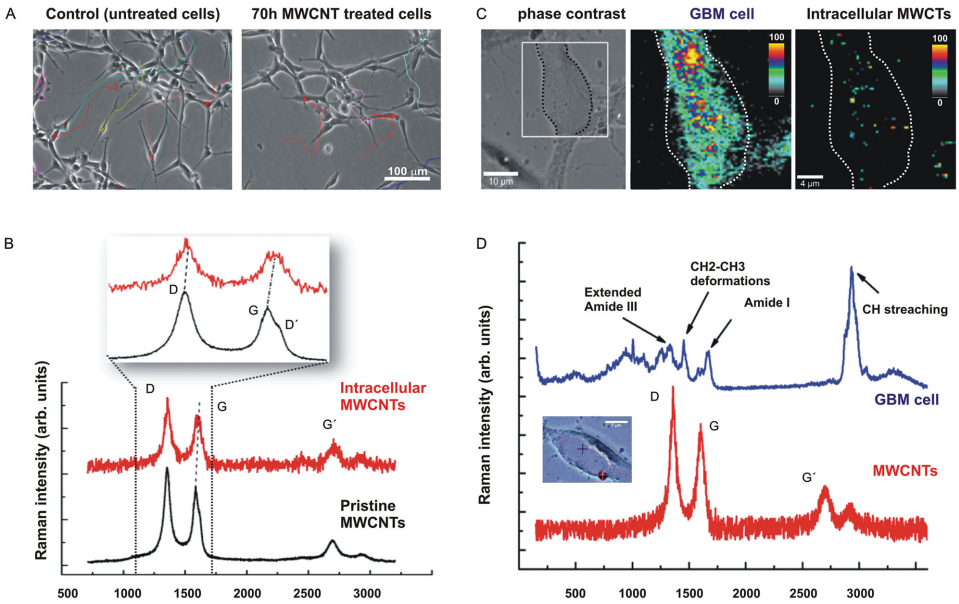

Figure 2. MWCNTs translocate into the cytoplasm of surgical specimen–derived cancer cells and interfere with cell spreading. A) Phase contrast microscopy images of the primary cultures of GBM cells obtained from surgical specimens. Both control and MWCNT-treated cells display a long bipolar morphology and no observable toxicity signs. Colored lines indicate 5 h cell trajectories. B) Comparison between the Raman spectra of pristine MWCNTs (black) and intracellular MWCNTs (red trace). These Raman spectra were obtained with a 532 nm line of a linear polarized frequency doubled Nd:YAG laser. The inset shows a detail of the typical fingerprints expected for MWCNTs spectral region corresponding to the D and G bands in order to point out the blue-shift of the Raman peak frequencies associated with the functionalization of the intracellular MWCNTs. Though only minor differences in the peak positions are observed, the spectrum of MWCNTs treated glioblastoma cell is slightly shifted to higher wavenumbers and a decrease in Raman intensities of D and, G and G′ modes are observed (Table S1, Supporting Information). C) Phase contrast image of a GBM cell captured through 100× objective of the confocal Raman microscope. (Center) Single confocal Z-plane Raman image of the same cell obtained integrating the intensities in the 2800–3000 cm^{-1} region (C–H stretching), integration time of 0.3 s × 10 accumulations, and a point spacing of 0.36 µm. (Right) Confocal Raman image obtained at the same confocal Z-plane to determine the localization of intracellular MWCNTs integrating the Raman intensities of the G band (1500–1700 cm^{-1} region). As shown in the color scale (indicating maximum/minimum CCD counts), bright yellow hues indicate the highest signals and gray hues low integrated G band intensities. D) Confocal Raman spectra of the cytoplasm of a MWCNT-treated GBM cell (inset, blue cross) and extracellular functionalized MWCNTs (inset, red cross). Integration time of 0.5 s × 10 accumulations and 0.3 s × 10 accumulations, respectively.

DOI: 10.1002/adhm.201500252

neural-derived cell lines and the primary GBM cell cultures with 0, 25, 50, and 75 μg mL^{-1} of MWCNTs in the growing medium for 70 h. Again, this analysis confirmed a statistically significant speed reduction, of up to 62%, with dosages of 50 μg mL^{-1} (Table S2, Supporting Information). Larger dosages (75 μg mL^{-1}) triggered a massive cytotoxic effect, suggesting excess MWCNTs probably interfere with some other critical cellular processes leading to cell death.

The interaction of nanomaterials with proteins or lipids, the actual biological building blocks, is still poorly understood as reviewed by Tay and colleagues.[34] These studies demonstrate that MWCNTs could play a pivotal role in cancer treatment in combination to standard therapies interfering with cancer cell migration. Other nanomaterials such as TiO_2, SiO_2, and hydroxyapatite nanoparticles have also been recently shown to interfere with cell migration damaging the microtubule network.[35] Our work demonstrates that MWCNTs could play a pivotal role in cancer treatment in combination to standard therapies interfering with cancer cell migration. We have previously documented the molecular interaction of MWCNTs with tubulin intracellularly,[11] and how the biomimetic properties of MWCNTs obstruct microtubule function during mitosis behaving as spindle poisons, same as traditional microtubule-binding drugs such as taxol. Remarkably, the interaction of MWCNTs with the microtubule is not site-specific. Instead MWCNTs appear to interact along the protofilament surface,[36] and this fact has two major advantages. First, MWCNTs do not require a specific binding site in the tubulin molecule subject of mutations. And second, the MWCNTs interaction with microtubules permits other microtubule-binding drugs to interact with their structural pocket in the tubulin molecule. Here we show how, in addition to the antiproliferative effect of MWCNTs, these nanomaterials also display important antimigratory effects in cancer cells. This new intrinsic feature of MWCNTs could significantly boost the mechanism of action of traditional microtubule-binding cytotoxic chemotherapies[16–18] and thus might serve to bypass some of the drug-resistance mechanisms in cancer cells.[37] Being metastasis the primary cause of death for most cancers, we believe these new properties of MWCNTs position these nanomaterials as a new ground-breaking type of future synthetic microtubule-stabilizing therapies that could play a pivotal role in future cancer treatment.

Experimental Section

MWCNTs Synthesis and Characterization: CNTs of 3–12 walls, with outer diameter ranging from 5 to 15 nm were synthesized following the catalytic chemical vapor deposition method using Co and Mo particles as catalyst.[38] An aqueous HCl treatment procedure was applied to clean and separate the MWCNTs from contaminants. The as-prepared MWCNTs were characterized by various techniques including Raman spectroscopy, transmission electron microscopy (TEM), and thermogravimetric analyses (TGA) (Figure S2, Supporting Information). MWCNTs produce a characteristic Raman spectrum distinguishable of SWCNTs spectrum revealing typical MWCNT resonances[39,40] such as the dispersive disorder induced D band at 1330 cm^{-1}, the tangential G band at 1586 cm^{-1}, and the D′ band at 1614 cm^{-1}. TEM was performed in a JEOL JEM 2100 microscope operating at 120 kV. Samples were prepared using ethanol as dispersant and omitting the sample centrifugation steps. A drop of this suspension was adsorbed onto a Lacey copper grid. The TGA was performed with a Perkin Elmer Pyris 1 system. Measurements were conducted by heating 9–12 mg of MWCNTs in dry air from 35 °C up to 1000 °C at a rate of 2 °C min^{-1}. TGA results showed a typical characteristic CNT curve where the oxidations of hexagonal carbon ring appeared at 550 °C. Qualitative information on the purity of CNT could be obtained from the TGA based on the extent of nonoxidizable residues at high temperature. In our measurements, catalytic metal impurities were not observed between 600 and 1000 °C. All these techniques confirmed the absence of undesired impurities in these MWCNTs samples.

MWCNTs Dispersion and Functionalization: CNTs were debundled and dispersed by repeated cycles of vortex mixing followed by mild sonication (3 min, frequency of 20 kHz, 130 W in a SONICS Vibracell VCX130) and centrifugation in cell culture medium (Dulbecco's modified Eagle medium (DMEM) from Sigma-Aldrich) containing serum and antibiotics as previously described.[10,11] The stability of the stock suspension was checked by centrifugation at 14 000 *g* after each sonication cycle. Visible absorption was used to determine MWCNT concentration in the 400–600 nm range. Further details of the stability and dispersion of MWCNTs in the cell culture medium can be found in previous work.[10,11] A total of 3–5 cycles were sufficient to obtain a well-dispersed concentrated suspension of MWCNTs which was rediluted in culture medium to the concentrations indicated in the text.

Confocal Raman Spectroscopy Imaging: A confocal Raman microscope (Alpha300, WITec) equipped with a piezo scanner and a linear polarized frequency doubled Nd:YAG laser (532 nm excitation wavelength) focused through an air objective (Nikon, 100×, NA = 0.9) was used. To avoid damage and heating, the laser power was controlled below 2 mW. The spatial resolution is diffraction limited. In the setup used, features at a distance of $r = 0.61 \times 532/0.9 = 0.36$ μm can be distinguished and completely resolved at a distance of 0.72 μm. Mapping was done for the stack scan with a step size of 0.36 μm in X/Y and a constant Z (depth) in a square of 23 × 25 μm on X/Y. To get a better signal-to-noise ratio, every spectrum was acquired with an integration time of 0.3 s, meaning $75 \times 75 = 5625$ spectra for one image. Images from this multispectra file were computed by integrating the appropriate Raman peaks using the ScanCtrlSpectroscopyPlus software (WITec, Germany). The images were constructed mapping the signals of G mode (1500–1700 cm^{-1}) and the C–H stretching in the 2800–3000 cm^{-1} region.[39,40]

Cell Culture, Cell Tracking, and Imaging Techniques: The human cancer cell line models used (HeLa, MCF7, SH-SY5Y, and U87MG) have been thoroughly characterized in the literature.[41-43] Primary GBM cell cultures have been previously characterized by our group.[24] Cells were grown in Dulbecco's Modified Eagle Medium containing 10% serum at 37 °C, 5% CO_2 and were exposed to 25 μg mL^{-1} MWCNTs concentration in the culture medium for 70 h (unless otherwise indicated). Controls and MWCNT-treated cells were grown on the same culture plate and were imaged simultaneously. Centrosomal trajectories were labeled by gene transfer with a vector expressing GFP:EB1 in HeLa cells 24 h before exposure to MWCNTs in the medium. This vector was kindly provided by Dr. Akhmanova (Utrecht University, The Netherlands). Nuclear DNA was labeled with Hoechst dye (bis-benzimide) (Sigma-Aldrich). Cell tracking analysis was performed on time-lapse video microscopy movies obtained @ 15 min/frame during 5 h on a Nikon Eclipse Ti live-cell station, using a 10× Nikon NA 0.45. Quantification analysis was performed with the NIS-Elements software. The average cell migration speed was obtained for a minimum of hundred cells in at least three sets of experiments for each condition. Actual numbers of analyzed cells are designated in Table 1 as degrees of freedom (DF). Unpaired two-tailed Student's *t*-test was used for the statistical evaluation of differences between control and treated cells. Probability (*p*) values are also shown.

Supporting Information

Supporting Information is available from the Wiley Online Library or from the author.

DOI: 10.1002/adhm.201500252

Acknowledgements

The authors are very grateful to L. Álvarez-Montes and J. Díaz-Gómez for their help and to the Nikon A1R Laser Microscopy Unit of the IDIVAL Institute. The authors also thank Dr. Baylo and Dr. Toporski of the WITec Company for their help with the confocal Raman imaging. This work was supported by the Spanish ISCIII-MINECO under Projects ref. PI13/01074, AES 2013, MAT2012-38664-C02-01; MALTA Consolider-Ingenio ref. CSD2007-00045, PI10/02002, AES 2010; and the Spanish ISCIII programs RTICC refs. RD06/0020/0074 and RD12/0036/0022. The authors especially thank Fundación Eugenio Rodríguez Pascual ("ayudas de investigación" 2014, ref. 02-H048-64003).

[1] S. Park, D. Srivastava, K. Cho, *Nano Lett.* **2003**, *3*, 1273.
[2] X. Shi, A. Von demBussche, R. H. Hurt, A. B. Kane, H. Gao, *Nat. Nanotechnol.* **2011**, *6*, 714.
[3] L. Lacerda, J. Russier, G. Pastorin, M. A. Herrero, E. Venturelli, H. Dumortier, K. T. Al-Jamal, M. Prato, K. Kostarelos, A. Bianco, *Biomaterials* **2012**, *33*, 3334.
[4] E. Mooney, P. Dockery, U. Greiser, M. Murphy, V. Barron, *Nano Lett.* **2008**, *8*, 2137.
[5] L. M. Sargent, A. F. Hubbs, S. H. Young, M. L. Kashon, C. Z. Dinu, J. L. Salisbury, S. A. Benkovic, D. T. Lowry, A. R. Murray, E. R. Kisin, K. J. Siegrist, L. Battelli, J. Mastovich, J. L. Sturgeon, K. L. Bunker, A. A. Shvedova, S. H. Reynolds, *Mutat. Res., Genet. Toxicol. Environ. Mutagen.* **2012**, *745*, 28.
[6] A. E. Porter, M. Gass, K. Muller, J. K. Skepper, P. A. Midgley, M. Welland, *Nat. Nanotechnol.* **2007**, *2*, 713.
[7] H. Ali-Boucetta, A. Nunes, R. Sainz, M. A. Herrero, B. Tian, M. Prato, A. Bianco, K. Kostarelos, *Angew. Chem. Int. Ed.* **2013**, *52*, 2274.
[8] X. Li, Y. Peng, X. Qu, *Nucl. Acids Res.* **2006**, *34*, 3670.
[9] H. Shams, B. D. Holt, S. H. Mahboobi, Z. Jahed, M. F. Islam, K. N. Dahl, M. R. Mofrad, *ACS Nano* **2014**, *8*, 188.
[10] J. C. Villegas, L. Álvarez-Montes, L. Rodríguez-Fernández, J. González, R. Valiente, M. L. Fanarraga, *Adv. Healthcare Mater.* **2014**, *3*, 424.
[11] L. Rodríguez-Fernández, R. Valiente, J. González, J. C. Villegas, M. L. Fanarraga, *ACS Nano* **2012**, *6*, 6614.
[12] F. Pampaloni, E. L. Florin, *Trends Biotechnol.* **2008**, *26*, 302.
[13] C. Z. Dinu, S. S. Bale, G. Zhu, J. S. Dordick, *Small* **2009**, *5*, 310.
[14] E. Nogales, M. Whittaker, R. A. Milligan, K. H. Downing, *Cell* **1999**, *96*, 79.
[15] T. Mitchison, M. Kirschner, *Nature* **1984**, *312*, 237.
[16] M. A. Jordan, L. Wilson, *Curr. Opin. Cell Biol.* **1998**, *1*, 123.
[17] D. R. Matson, P. T. Stukenberg, *Mol. Interventions* **2011**, *11*, 141.
[18] J. Zhou, P. Giannakakou, *Curr. Med. Chem. Anti-Cancer Agents* **2005**, *5*, 65.
[19] L. Gonzalez, I. Decordier, M. Kirsch-Volders, *Biochem. Soc. Trans.* **2010**, *38*, 1691.
[20] G. W. Luxton, G. G. Gundersen, *Curr. Opin. Cell Biol.* **2011**, *23*, 579.
[21] E. Van Beneden, *Arch. Biol.* **1883**, *4*, 265.
[22] R. Li, G. G. Gundersen, *Nat. Rev. Mol. Cell Biol.* **2008**, *9*, 860.
[23] a) A. Béduer, F. Seichepine, E. Flahaut, I. Loubinoux, L. Vaysse, C. Vieu, *Langmuir* **2012**, *28*, 17363; b) A. Béduer, F. Seichepine, E. Flahaut, I. Loubinoux, L. Vaysse, C. Vieu, *Langmuir* **2012**, *28*, 17363.
[24] P. Ruiz-Ontañon, J. L. Orgaz, B. Aldaz, A. Elosegui-Artola, J. Martino, M. T. Berciano, J. A. Montero, L. Grande, L. Nogueira, S. Diaz-Moralli, A. Esparís-Ogando, A. Vazquez-Barquero, M. Lafarga, A. Pandiella, M. Cascante, V. Segura, J. A. Martinez-Climent, V. Sanz-Moreno, J. L. Fernandez-Luna, *Stem Cells* **2013**, *31*, 1075.
[25] M. J. O'Connell, S. M. Bachilo, C. B. Huffman, V. C. Moore, M. S. Strano, E. H. Haroz, K. L. Rialon, P. J. Boul, W. H. Noon, C. Kittrell, J. Ma, R. H. Hauge, R. B. Weisman, R. E. Smalley, *Science* **2002**, *297*, 593.
[26] D. A. Heller, P. W. Barone, J. P. Swanson, R. M. Mayrhofer, M. S. Strano, *J. Phys. Chem. B* **2004**, *108*, 6905.
[27] M. S. Strano, C. B. Huffman, V. C. Moore, M. J. O'Connell, E. H. Haroz, J. Hubbard, M. Miller, K. Rialon, C. Kittrell, S. Ramesh, R. H. Hauge, R. E. Smalley, *J. Phys. Chem. B* **2003**, *107*, 6979.
[28] E. Joselevich, H. Dai, J. Liu, K. Hata, A. H. Windle, *Carbon Nanotubes, Topics in Applied Physics*, Vol. *111* (Eds: A. Jorio, D. S. Dresselhaus, G. Dresselhaus), Springer-Verlag, Germany **2008**.
[29] S. F. Chin, R. H. Baughman, A. B. Dalton, G. R. Dieckmann, R. K. Draper, C. Mikoryak, I. H. Musselman, V. Z. Poenitzsch, H. Xie, P. Pantano, *Exp. Biol. Med.* **2007**, *232*, 1236.
[30] M. S. Arnold, M. O. Guler, M. C. Hersam, S. I. Stupp, *Langmuir* **2005**, *21*, 4705.
[31] G. R. Dieckmann, A. B. Dalton, P. A. Johnson, J. Razal, J. Chen, G. M. Giordano, E. Muñoz, I. H. Musselman, R. H. Baughman, R. K. Draper, *J. Am. Chem. Soc.* **2003**, *125*, 1770.
[32] S. S. Karajanagi, H. C. Yang, P. Asuri, E. Sellitto, J. S. Dordick, R. S. Kane, *Langmuir* **2006**, *22*, 1392.
[33] W. J. Huang, S. Taylor, K. Fu, Y. Lin, D. Zhang, T. W. Hanks, A. M. Rao, Y. P. Sun, *Nano Lett.* **2002**, *2*, 311.
[34] C. Y. Tay, M. I. Setyawati, J. Xie, J. W. Parak, D. T. Leong, *Adv. Funct. Mater.* **2014**, *24*, 5936.
[35] C. Y. Tay, P. Cai, M. I. Setyawati, W. Fang, L. P. Tan, C. H. Hong, X. Chen, D. T. Leong, *Nano Lett.* **2014**, *14*, 83.
[36] L. García Hevia, F. Fernández, C. Grávalos, A. García, J. C. Villegas, M. L. Fanarraga, *Nanomedicine* **2014**, *9*, 1581.
[37] G. A. Orr, P. Verdier-Pinard, H. McDaid, S. B. Horwitz, *Oncogene* **2003**, *22*, 7280.
[38] E. Flahaut, C. H. Laurent, A. Peigney, *Carbon* **2005**, *43*, 375.
[39] S. Dresselhaus, G. Dresselhaus, R. Saito, A. Jorio, *Phys. Rep.* **2005**, *409*, 47.
[40] P. R. Griffiths, E. V. Miseo, *Infrared and Raman Instrumentation for Mapping and Imaging* (Eds: R. Salzer, H. W. Siesler), Wiley-VCH, Weinheim, Germany **2009**, pp 1–64
[41] H. D. Soule, J. Vazguez, A. Long, S. Albert, M. Brennan, *Natl. Cancer. Inst.* **1973**, *51*, 1409.
[42] H. R. Xie, L. S. Hu, G. Y. Li, *Chin. Med. J.* **2010**, *123*, 1086.
[43] M. J. Clark, N. Homer, B. D. O'Connor, Z. Chen, A. Eskin, H. Lee, B. Merriman, S. F. Nelson, *PLoS Genet.* **2010**, *6*, e1000832.

DOI: 10.1002/adhm.201500252